Time history analysis of seismic response of through CFST non isolated and isolated arch bridges

Zhonghu Gao[1], Weigang Sun[2]
[1]School of Civil Engineering, Northwest Minzu University, Lanzhou, China
[2]School of Civil Engineering, Shijiazhuang Tiedao University, Shijiazhuang, China
[1]Corresponding author
E-mail: [1]*gzhh@xbmu.edu.cn*, [2]*swagan@163.com*

Received 1 April 2022; received in revised form 13 June 2022; accepted 7 July 2022
DOI https://doi.org/10.21595/jve.2022.22561

Abstract. To explore the difference in the impact of transverse bracing on the seismic effect of through concrete-filled steel tube arch bridges with non-isolated and earthquake-isolated, nine non-isolated and earthquake-isolated structural models under different cross-bracing arrangements were established, and Elcentro seismic waves were selected. The internal force, displacement, velocity, absolute acceleration, relative acceleration, and separation of arch ribs of each model were compared and analyzed under uniform excitation along the bridge, transverse and vertical directions, multi-dimensional combined excitation, and multipoint excitation considering the traveling wave effect. Based on the shear force and displacement of the earthquake support, it is concluded that the internal force response of different excitations of various models is more complicated. The installation of transverse bracing on the upper part of the arch rib can reduce the vertical displacement of the arch rib of the nonseismic structure. The "X"-shaped cross brace at the top of the arch rib and the "K"-shaped cross brace at the lower part help to reduce the transverse acceleration of the arch rib. The absolute acceleration and relative acceleration of the seismic structure arch ribs are significantly reduced.

Keywords: transverse bracing, seismic isolation, through concrete-filled steel tube arch bridge, time history analysis.

1. Introduction

In recent years, there have been frequent earthquakes around the world. As a lifeline project for postdisaster reconstruction and disaster relief, bridges have always received extensive attention. A large number of concrete-filled steel tube arch bridges have been built, and research on related cross-bracing arrangements is also ongoing.

Dong Rui et al. [1] studied the effectiveness of new L-shaped cross-braces in the stability of long-span concrete-filled steel tube truss arch bridges. Hejiang Third Bridge was taken as the engineering background, using a combination of numerical calculation and theoretical analysis to compare and analyze its mechanical performance and stability, and use orthogonal experiment and variance analysis methods to evaluate the significance of L-shaped cross braces in the stability of long-span CFST truss arch bridges Zhang Sumei and Yundi [2] analyzed and compared the possible layout schemes of cross braces and X braces for a 360-meter-span half-through concrete-filled steel tube arch bridge, and proposed the rationality of X braces and cross braces accordingly. According to the principle of equal bracing area and similar material consumption of transverse bracing system, four bracing schemes were proposed and analyzed for ultimate bearing capacity respectively; Wan Peng et al. [3] designed the Guangzhou Xinguang Bridge with a main span of 428 meters in plan, the large-scale finite element software ANSYS was used to establish a three-dimensional finite element model of the full bridge, and the influence of the number and position of the transverse braces on the elastic stability and the ultimate bearing capacity of the plane was analyzed. Jin Bo et al. [4] used the finite element method to analyze the influence of transverse bracing on the overall stability of a cable-stayed concrete-filled steel tube arch bridge; Chen Baochun et al. [5] found arch and arch-girder composite bridges are the main ones; Liu Zhao et al. [6] derived the analytical calculation formula for the lateral elastic stability bearing capacity of arch bridges with transverse braces based on the energy principle, and verified the proposed finite element numerical solution through a numerical example. The correctness of the analytical formula and finally discussed the influence of structural parameters on the stability of bearing capacity; Wu Meirong et al. [7] stepped into the non-thrust half-through concrete-filled steel tube arch bridge in terms of rise-span ratio, width-span ratio, main arch rib stiffness, transverse bracing Changes in the dynamic characteristics of the bridge structure when the layout mode, suspender failure, and support layout are changed; Kong Dandan et al.[8] took a steel truss arch bridge in a certain city as the research object and showed that increasing the number of wind bracing structures can significantly improve the structure's performance stability; but when the number of wind bracing is sufficient, the continue to increase the number of wind bracing structures, the stability of the structure cannot be greatly improved, and the setting of diagonal braces has a great influence on the overall stability, especially "K" and "X" diagonal braces have a significant impact on the structural stability; Li Xiayuan et al. [9] relying on a certain through-type steel tube concrete arch bridge, based on the original bridge wind bracing form, using the MIDAS Civil finite element analysis software to establish the "-" The calculation model for the through-type steel tube concrete arch bridge with "X"-shaped wind bracing, "K"-shaped wind bracing, "m"-shaped wind bracing, and "X"-shaped wind bracing, extracts the first 20-order natural frequency and The vibration mode types of the first 6 steps were compared and analyzed with the original bridge; Zheng Xiaoyan et al. [10] studied the stability of the tied arch bridge during the construction phase and the influence of temporary transverse bracing on the structural stability.

In this paper, nine non-isolated and earthquake-isolated structural models under different cross-bracing arrangements were established, and Elcentro seismic waves were selected. The internal force, displacement, velocity, absolute acceleration, relative acceleration, and separation of arch ribs of each model were compared and analyzed under uniform excitation along the bridge, transverse and vertical directions, multi-dimensional combined excitation, and multipoint excitation considering the traveling wave effect.

The layout position and layout of the transverse bracing have different effects on the through-type concrete-filled steel tube seismic arch bridge and the seismic isolation arch bridge. The article will conduct comparative analysis and research to provide the necessary references for the design and construction of similar arch bridges.

2. Principles of time history analysis

The vibration equation for dynamic time history analysis is:

$$[M]\{\ddot{y}\}+[C]\{\dot{y}\}+[K]\{y\}=\{P\}, \tag{1}$$

where M_S, C_S, K_S denote the mass matrix, damping matrix and stiffness matrix of the corresponding structural non-supporting position, respectively, use M_b, C_b, K_b to denote the mass matrix, damping matrix and stiffness matrix of the corresponding structural support position, respectively, and use $\ddot{y}_s$, $\dot{y}_s$, y_s to denote the structural non-supporting position under earthquake action, the acceleration, velocity and absolute displacement of the support, with $\ddot{y}_b$, $\dot{y}_b$, y_b, respectively represent the acceleration, velocity and absolute displacement vector of the structural support position under the action of an earthquake. F_b is the reaction force of the support under the action of an earthquake. Then the vibration equation can be expressed in the following form:

$$\begin{bmatrix} M_{ss} & 0 \\ 0 & M_{bb} \end{bmatrix}\begin{Bmatrix} \ddot{y}_s \\ \ddot{y}_b \end{Bmatrix}+\begin{bmatrix} C_{ss} & C_{sb} \\ C_{bs} & C_{bb} \end{bmatrix}\begin{Bmatrix} \dot{y}_s \\ \dot{y}_b \end{Bmatrix}+\begin{bmatrix} K_{ss} & K_{sb} \\ K_{bs} & K_{bb} \end{bmatrix}\begin{Bmatrix} y_s \\ y_b \end{Bmatrix}=\begin{bmatrix} 0 \\ F_b \end{bmatrix}. \tag{2}$$

3. Finite element model

Taking an actual through arch bridge as the background, nine non-seismic and seismic finite element models of different transverse bracing arrangements are established. The transverse bracing arrangement and finite element model are shown in Table 1 and Fig. 1. The seismic isolation model is equipped with lead-core rubber seismic isolation bearings, and the bearing parameters are shown in Table 2. The bridge has a main span of 127 m and a bridge deck width of 31 m. The arch rib cross-section is dumbbell-shaped. The diameter of the upper and lower arch ribs is 1.2 m, and the diameter of the cross brace is 1.3 m.

Table 1. The layout of transverse bracing in various working conditions

Working condition 1	Working condition 2	Working condition 3	Working condition 4	Working condition 5	Working condition 6	Working condition 7	Working condition 8	Working condition 9
A cross brace in the shape of “-” on the vault	Three “-”-shaped cross braces on the vault and the middle and upper parts	Three “-”-shaped cross braces on the vault and the middle and lower parts	Five-way "-" cross brace	One “-”-shaped cross brace on the vault, and two “K” cross braces in the middle and upper part	One “-”-shaped cross brace on the vault, two “K” cross braces in the middle and lower part	The vault has one “-”-shaped cross brace and four “K”-shaped cross braces	One “-”-shaped cross brace on the vault and four “X” cross braces	Five “X”-shaped cross braces

Table 2. Parameter table of lead rubber bearing

Support plane size (mm×mm)	Lead core yield (kN)	Rigidity before yielding (kN/mm)	Rigidity after yielding (kN/mm)	Horizontal equivalent stiffness (kN/mm)
1320×1320	964	25.6	3.9	6.4

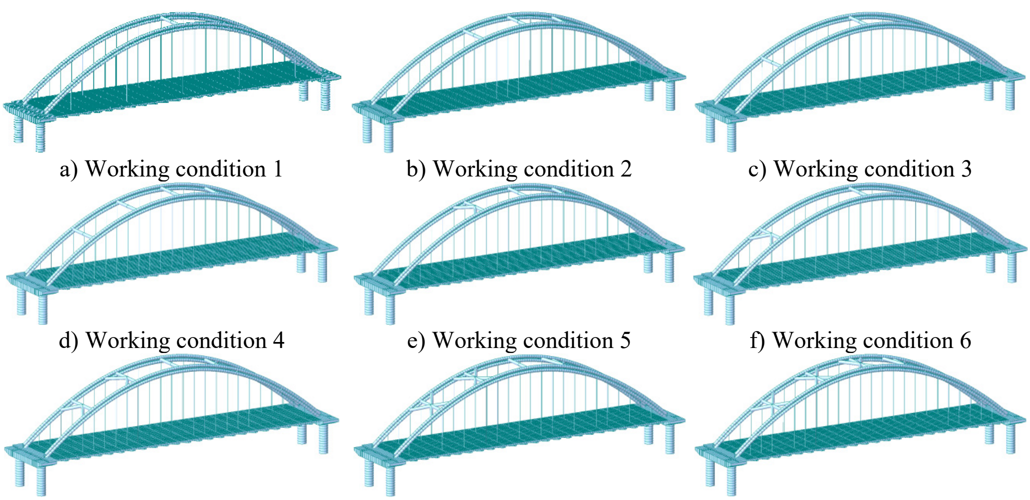

a) Working condition 1 b) Working condition 2 c) Working condition 3
d) Working condition 4 e) Working condition 5 f) Working condition 6
g) Working condition 7 k) Working condition 8 l) Working condition 9

Fig. 1. Finite element model diagram

4. Analysis of dynamic characteristics

Through the finite element software analysis of the dynamic characteristics, the frequency and mode shape of the non-isolated and isolated models under nine working conditions are obtained. The first three orders are shown in Table 3, and the frequency comparison is shown in Fig. 2. It can be seen that the first-order modes of the two models under nine working conditions are all arch rib lateral inclination, and the first-order frequencies of working conditions 1, 2, 3, and 4 have little difference, while the first-order frequencies of working conditions 8 and 9 are relatively different. Large "K"-shaped cross braces and "X" cross braces can increase the fundamental frequency, and the effect of being close to the lower part of the arch rib is obvious. The "X" cross brace on the dome actually reduces the fundamental frequency. The second and third order frequencies and modes of the two models are quite different, and the influence of the cross bracing of the non-isolated model is more obvious than that of the isolated model.

Table 3. The first third-order frequency and mode shape of each working condition

Working condition	Types	Frequency and mode shape	First order	Second order	Third order
Working condition 1	Non-isolated	Mode shape	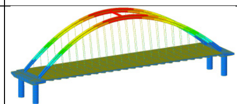	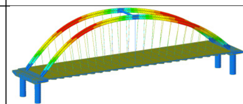	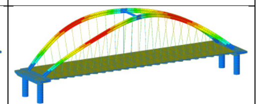
		Frequency	0.167	0.520	0.521
	isolation	Mode shape	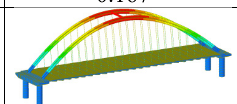	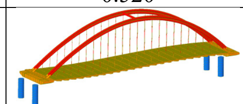	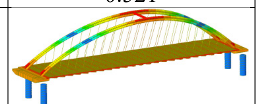
		Frequency	0.160	0.253	0.283
Working condition 2	Non-isolated	Mode shape	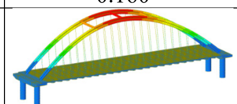	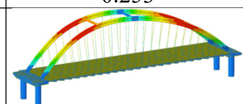	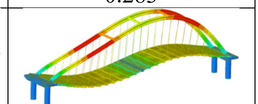
		Frequency	0.167	0.517	0.647
	isolation	Mode shape	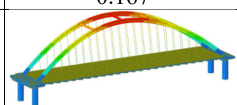	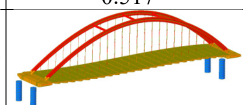	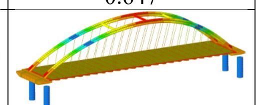
		Frequency	0.160	0.252	0.284
Working condition 3	Non-isolated	Mode shape	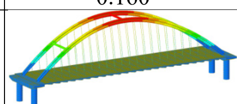	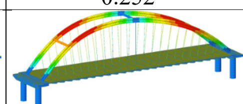	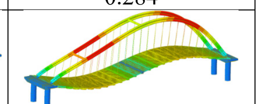
		Frequency	0.168	0.518	0.647
	isolation	Mode shape	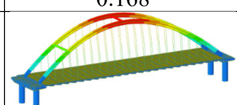	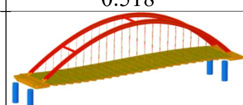	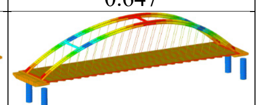
		Frequency	0.161	0.252	0.284
Working condition 4	Non-isolated	Mode shape	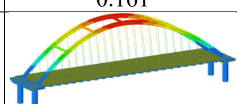	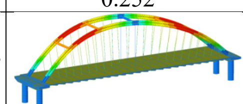	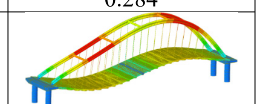
			0.168	0.515	0.645
	isolation	Mode shape	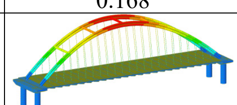	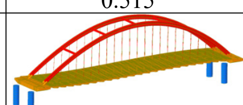	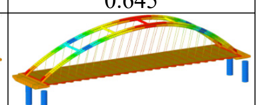
		Frequency	0.161	0.252	0.284
Working condition 5	Non-isolated	Mode shape	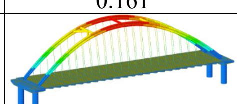	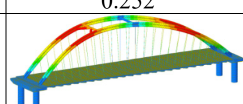	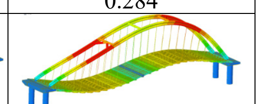
		Frequency	0.188	0.522	0.645
	isolation	Mode shape	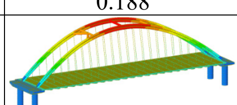	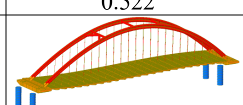	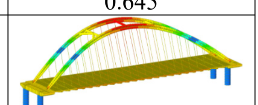
		Frequency	0.177	0.252	0.290

Working condition 6	Non-isolated	Mode shape	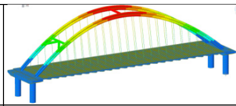	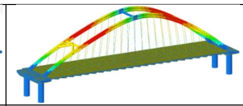	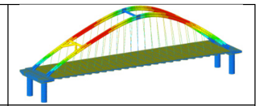
		Frequency	0.213	0.546	0.645
	isolation	Mode shape	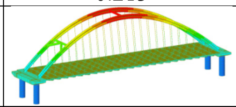	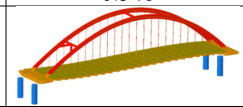	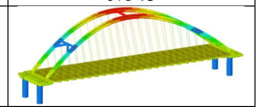
		Frequency	0.195	0.252	0.297
Working condition 7	Non-isolated	Mode shape	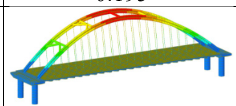	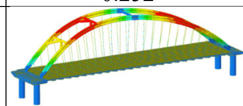	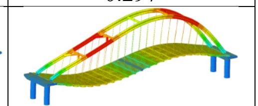
		Frequency	0.231	0.548	0.642
	isolation	Mode shape	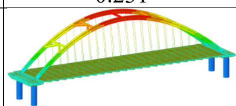	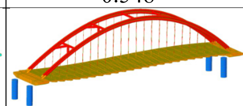	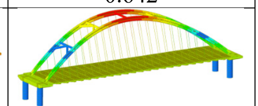
		Frequency	0.205	0.252	0.306
Working condition 8	Non-isolated	Mode shape	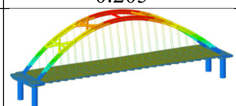	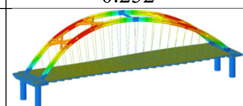	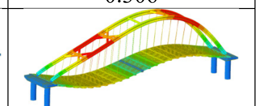
		Frequency	0.332	0.619	0.640
	isolation	Mode shape	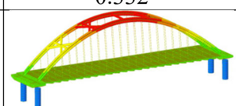	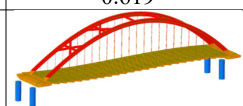	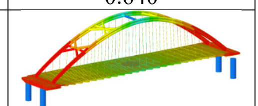
		Frequency	0.233	0.251	0.363
Working condition 9	Non-isolated	Mode shape	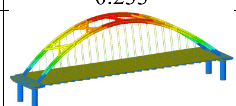	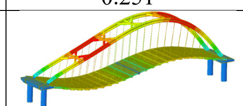	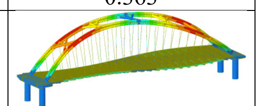
		Frequency	0.330	0.640	0.691
	isolation	Mode shape	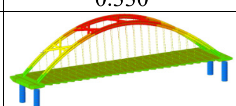	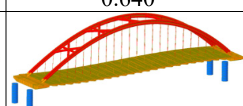	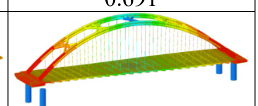
		Frequency	0.232	0.251	0.365

5. Selection of seismic wave and apparent wave speed

The seismic fortification intensity of the area where the bridge is located is 8 degrees (0.2 g), and the site category is Type II. The El Centro seismic wave is selected, and the peak acceleration value of the seismic wave is multiplied by a coefficient of 0.339 for adjustment. The adjusted seismic wave is shown in Fig. 3, and the action time is taken as 20 s, the excitation direction is uniform excitation along the bridge direction, uniform excitation across the bridge direction, uniform excitation vertical direction, multi-dimensional combination one (long bridge direction + 0.3 horizontal bridge direction + 0.3 vertical) excitation, multi-dimensional combination two (0.3 forward bridge direction + Transverse bridge direction + 0.3 vertical direction) excitation, multi-dimensional combination three (0.3 along bridge direction + 0.3 transverse bridge direction + vertical direction) excitation and the apparent wave speed is 100 m/s, 200 m/s, 300 m/s, 400 m/s, Multi-point excitation of 500 m/s, 1000 m/s, 1500 m/s, 2000 m/s.

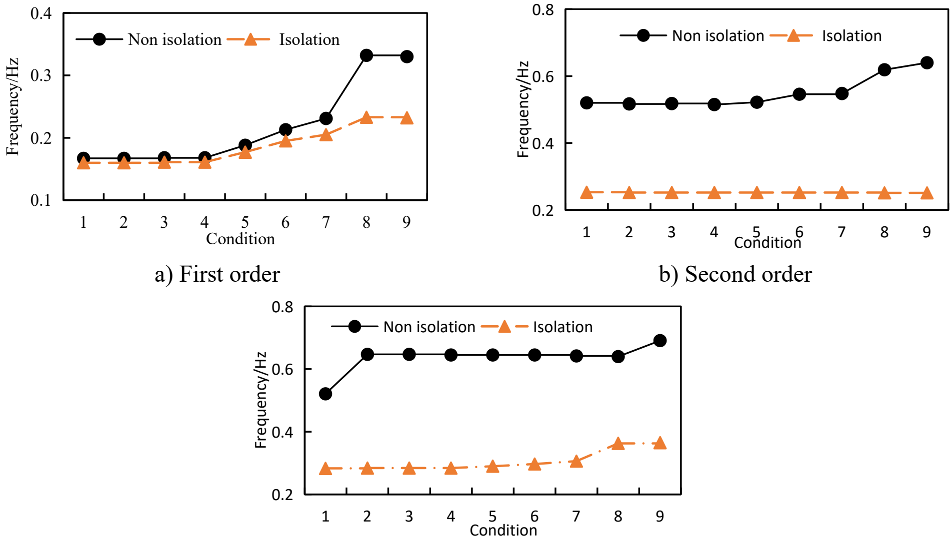

a) First order

b) Second order

c) Third order

Fig. 2. Frequency comparison

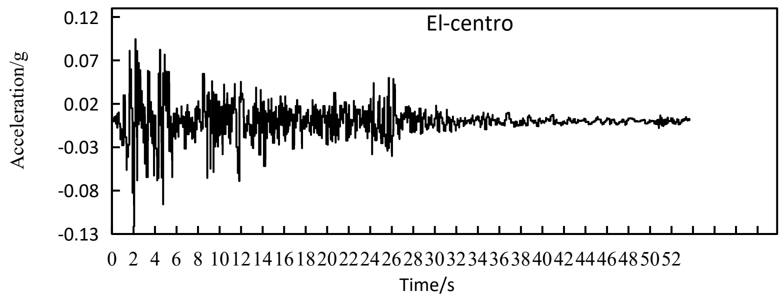

Fig. 3. El-centro seismic wave adjusted

6. Earthquake response analysis

6.1. Internal force of arch rib

See Table A1 for the maximum internal force and damping rate of arch ribs in different models under uniform excitation. See Table A2 for the maximum internal force and damping rate of arch ribs in different models under multi-dimensional combined excitation. Under multi-point excitation considering traveling wave effect, the maximum internal force and shock absorption rate of arch ribs in different models under various working conditions are shown in Table A3. The time-history response of partial arch foot axial force is shown in Fig. 4.

Through the comparison of Table A1 to Table A3 and Fig. 4, we can get:

(1) Under the action of seismic waves with different wave speeds in the bridge direction, transverse bridge direction, combination 1 and bridge direction, the main internal force of the seismic isolation structure arch rib in each working condition is significantly reduced;

(2) Under the action of vertical earthquake, the main internal forces of the seismic isolation structure arch ribs in various working conditions increased, the shear force F_Z increased by more than twice, and the bending moment M_y increased by more than three times;

(3) Under the action of the second combination earthquake, the arch rib axial force of each working condition of the seismic isolation structure decreases, the shear force F_z increases, the

bending moment M_z in working condition 8 and 9 increase, and the rest decrease. Under the action of the combination three earthquakes. The main internal force of the arch rib of the seismic isolation structure in the working condition increased, the shear force F_Z increased more than doubled, and the bending moment M_y increased more than doubled;

(4) Under the effects of lateral earthquake and combination, the main internal force of the seismic isolation structure arch ribs in working conditions 8 and 9 increase significantly.

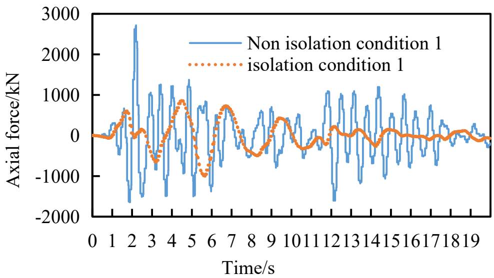

a) Working condition1 along the bridge

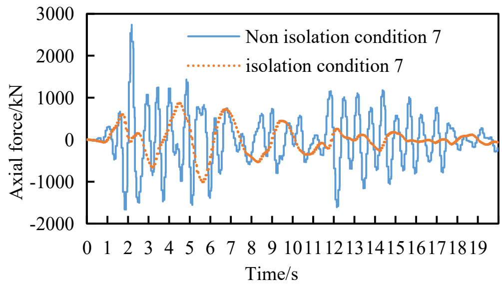

b) Condition 7 along the bridge

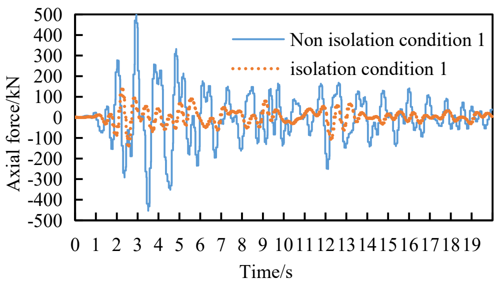

c) Condition 1 Cross-bridge direction

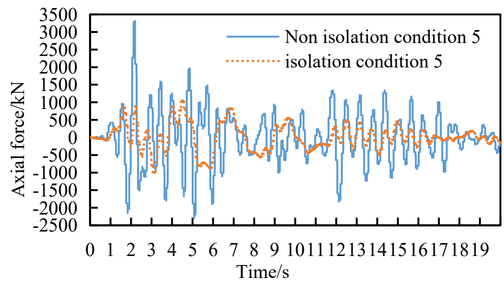

d) Working condition 5 Combination one

Fig. 4. Time history response of arch foot axial force

6.2. Arch rib displacement

The maximum displacement of the arch rib under transverse excitation is shown in Table 4, and the time-history response of the DY time history of the vault displacement under non-seismic conditions is shown in Fig. 5.

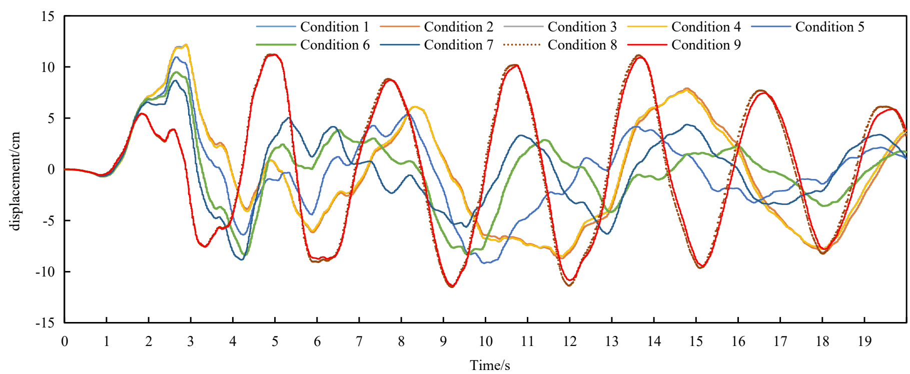

Fig. 5. DY time-history response of vault displacement under various conditions of non-seismic isolation

Through the comparative analysis of Table 4 and Fig. 5, we can get:

(1) Under the action of transverse bridge seismic wave, the arch ribs of non-seismic and

isolation models mainly undergo lateral displacement. The lateral displacements of working conditions 1, 2, 3, and 4 are not much different. The lateral displacements of working conditions 5, 6, and 7 are more than other, the working condition is small, and it is concluded that the “K”-shaped cross brace is better than the “-” cross brace and the “meter” cross brace in reducing the lateral displacement of the arch rib;

(2) Comparing various working conditions, it can be concluded that setting up transverse bracing on the upper part can reduce the vertical displacement of the arch rib of the non-seismic model.

Table 4. Arch rib displacement (unit: cm)

Incentive direction	Displacement direction	Model	Working condition								
			1	2	3	4	5	6	7	8	9
Cross bridge	Along the bridge	Non-isolated	0.220588	0.217772	0.218886	0.216088	0.19172	0.215155	0.190403	0.234662	0.238253
		Vertical Horizontal Vertical Isolated	0.095618	0.095142	0.095793	0.095229	0.08672	0.090369	0.097304	0.14055	0.138715
	Cross bridge	Non-isolated	12.178108	12.190638	12.160166	12.177714	10.963965	9.490335	8.852437	11.574302	11.437827
		Vertical Horizontal Vertical Isolated	13.456979	13.433771	13.436001	13.414679	12.387384	11.74146	10.855834	17.104378	16.846004
	Vertical	Non-isolated	0.575183	0.569438	0.572487	0.566709	0.505177	0.567788	0.505335	0.55977	0.564412
		Isolated	0.225666	0.225264	0.225162	0.224671	0.19714	0.210035	0.216076	0.3417	0.344369

6.3. Arch rib speed

The maximum speed of arch ribs under transverse excitation is shown in Table 5. The time-history response of the transverse velocity of the vault under each condition of seismic isolation is shown in Fig. 6. Through the comparative analysis of Table 5 and Fig. 6, we can get:

(1) Under the action of transverse bridge seismic waves, the lateral velocity of arch ribs in non-seismic and seismic isolation models basically increases in working conditions 1 to 8, while working condition 9 decreases slightly;

(2) Under the action of transverse bridge seismic waves, the longitudinal and vertical speeds of arch ribs in non-seismic and seismic models are relatively small in condition five;

(3) The speed of the arch ribs of the seismic isolation structure in each working condition is reduced.

Table 5. Arch rib speed (unit: cm/s)

Incentive direction	Speed direction	Model	Working condition 1	2	3	4	5	6	7	8	9
Cross bridge	Along the bridge	Non-isolated	1.572553	1.573233	1.55233	1.555467	1.481314	1.592136	1.495981	1.442885	1.443201
		Isolated	0.8401	0.842009	0.831214	0.836434	0.801512	0.875925	0.845275	0.88414	0.885579
	Cross bridge	Non-isolated	25.172737	25.105125	25.468387	25.328813	27.179484	29.70583	31.043626	39.780206	38.68521
		Isolated	19.793487	19.782502	19.837443	19.837609	18.940581	23.446982	26.028057	39.182534	38.69969
	Vertical	Non-isolated	3.808268	3.734763	3.786084	3.709999	3.400459	3.806481	3.455232	3.459467	3.521407
		Isolated	1.711642	1.729262	1.698642	1.715102	1.625263	1.767564	1.702519	1.688422	1.690779

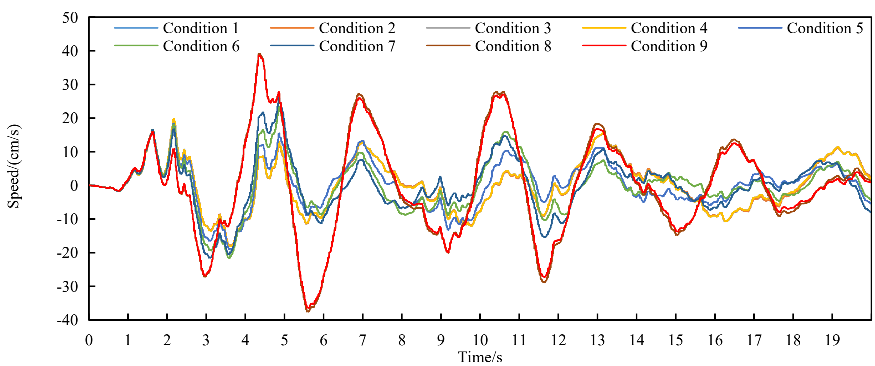

Fig. 6. Time-history response of vault lateral velocity in each case of seismic isolation

6.4. Absolute acceleration of arch rib

The maximum absolute acceleration of the arch rib under transverse excitation is shown in Table 6, and the time-history response of the lateral acceleration of the nine vaults under working conditions is shown in Fig. 7. Through the comparative analysis of Table 6 and Fig. 7, it can be obtained:

(1) Under the action of the transverse bridge seismic wave, the non-isolated and isolated model arch rib lateral acceleration, the non-seismic structure working condition 5 and working condition

7 are smaller, the seismic isolation structure working condition 7 is relatively small, and the working condition 9 is relatively small. Working condition 8 is reduced, it can be inferred that the "米"-shaped cross brace at the top of the arch rib, and the "K"-shaped cross brace at the lower part will help reduce the absolute acceleration of the arch rib.

(2) The absolute acceleration of the arch rib of the seismic isolation structure in each working condition is significantly reduced.

Table 6. Absolute acceleration of arch ribs (unit: cm/s^2)

Incentive direction	Absolute acceleration direction	Model	Working condition								
			1	2	3	4	5	6	7	8	9
Cross bridge	Cross bridge	Non-isolated	302.069666	298.588074	314.635446	306.619751	291.123396	315.517481	291.100165	343.150259	338.930472
		Isolated	83.273905	82.935068	82.92821	83.290524	82.154905	81.068172	79.804811	91.825414	88.816718

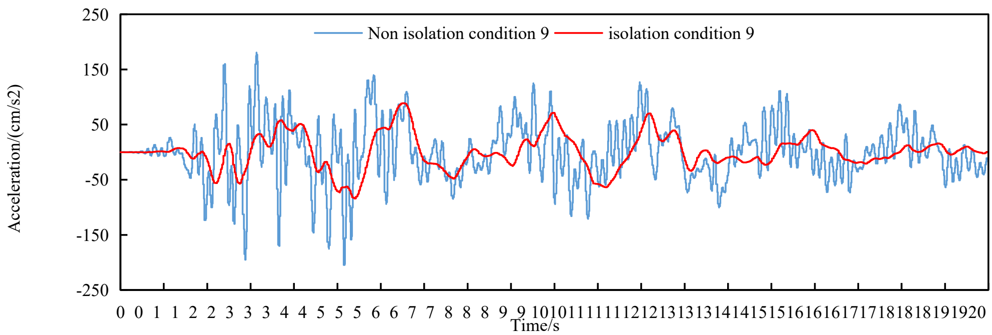

Fig. 7. Time-history response of lateral acceleration of nine vaults under working conditions

6.5. Relative acceleration of arch rib

The maximum relative acceleration of arch ribs under transverse excitation is shown in Table 7.

Table 7. Relative acceleration of the arch ribs (unit: cm/s^2)

Incentive direction	Relative acceleration direction	Model	Working condition								
			1	2	3	4	5	6	7	8	9
Cross bridge	Cross bridge	Non-isolated	350.799422	353.664181	349.011316	349.716454	351.965781	330.543943	325.231323	348.104201	346.062742
		Isolated	157.707118	157.621842	157.721081	157.612437	156.244506	156.104435	154.734779	150.697906	151.129868

Through the comparative analysis of Table 7, we can get:

(1) Under the action of the transverse bridge seismic wave, the relative acceleration of the arch ribs of the non-seismic and isolation models is relatively small for the non-seismic structure working conditions 6 and 7, and the seismic isolation structure working conditions 1 to 7 basically show a decreasing trend;

(2) The relative acceleration of the arch rib of the seismic isolation structure in each working condition is significantly reduced.

6.6. Shear force and displacement of seismic isolation support

See Table 8 for the maximum shear force and displacement of the seismic isolation support. See Fig. 8 for the shear force comparison of some supports. See Fig. 9 for the displacement comparison of some supports.

Table 8. Maximum shear force and displacement of seismic isolation support

Incentive direction	Working condition	1	2	3	4	5	6	7	8	9
Along the bridge	Shear force / kN	940.21	939.78	939.62	940.56	940.73	940.49	939.69	938.43	938.22
	Displacement / cm	4.87	4.87	4.86	4.90	4.90	4.90	4.89	4.84	4.84
Cross bridge	Shear force / kN	873.87	873.54	873.76	873.44	861.16	844.86	843.41	762.70	753.41
	Displacement / cm	4.34	4.33	4.34	4.33	4.23	4.09	3.95	3.40	3.35
Vertical	Shear force / kN	190.50	190.67	190.48	190.66	190.81	190.56	190.93	191.25	191.63
	Displacement / cm	0.75	0.75	0.75	0.75	0.75	0.75	0.75	0.75	0.76
Combination one	Shear force / kN	934.84	937.98	937.77	936.80	934.97	936.03	937.64	938.89	938.63
	Displacement/cm	4.97	4.99	5.00	5.01	4.98	4.98	4.96	4.94	4.91
Combination two	Shear force / kN	852.10	851.64	855.63	852.19	837.90	822.17	815.99	745.03	741.08
	Displacement / cm	4.37	4.38	4.41	4.37	4.22	4.18	3.91	3.45	3.34
Combination three	Shear force / kN	448.11	450.55	448.51	452.70	440.66	442.84	446.90	442.42	442.31
	Displacement / cm	1.88	1.84	1.84	1.81	1.88	1.85	1.85	1.86	1.86

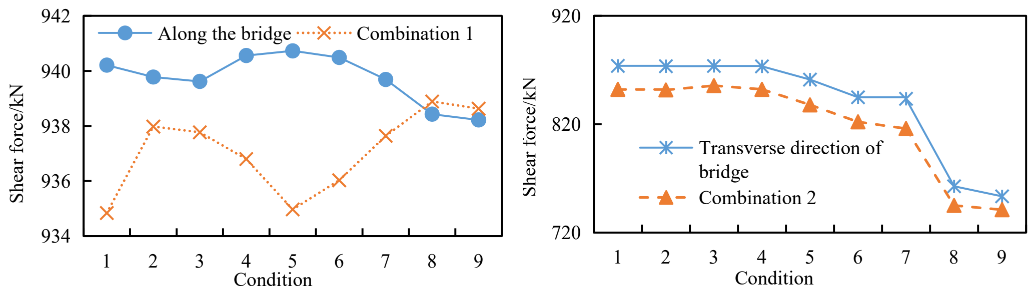

a) Along the bridge and combination one b) Cross-bridge direction and combination two

Fig. 8. Comparison of bearing shear force

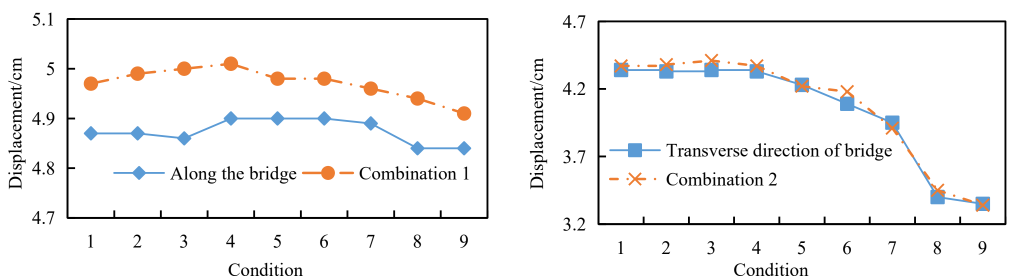

a) Along the bridge and combination one b) Cross-bridge direction and combination two

Fig. 9. Comparison of bearing displacement

See Figure 10 for the shear response time history of some supports. Hysteresis curve for some supports. See Fig. 11. From the analysis of Table 8 and Fig. 8 to Fig. 11, we can get:

(1) The maximum shear force of the seismic isolation support under the excitation of working conditions 1 to 7 is greater than that of combination 1, and the maximum shear force of the seismic isolation support under the excitation of working conditions 8 and 9 is greater than the excitation of the forward bridge;

(2) Under the action of the transverse bridge direction and combination two, the maximum shear force of the seismic isolation support of working conditions 1 to 9 shows a decreasing trend, and the linear direction is basically similar, and the transverse bridge excitation of each working condition is greater than the combination two excitation;

(3) The maximum displacement of each working condition is that the excitation of combination one is greater than the excitation along the bridge direction, and the cross-bridge direction and combination two are basically the same, and there is a decreasing trend from working condition 1 to working condition 9;

Under the vertical excitation, the shear force and displacement of all working conditions are basically the same.

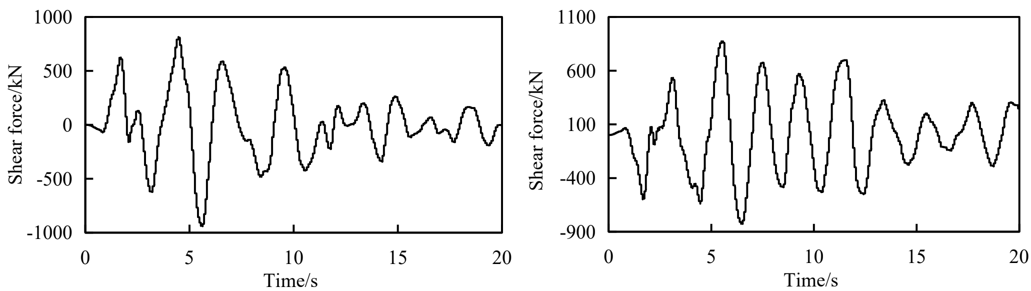

a) Working condition 5, along the bridge direction excitation
b) Working condition 1 cross-bridge excitation

Fig. 10. Time history response of bearing shear force

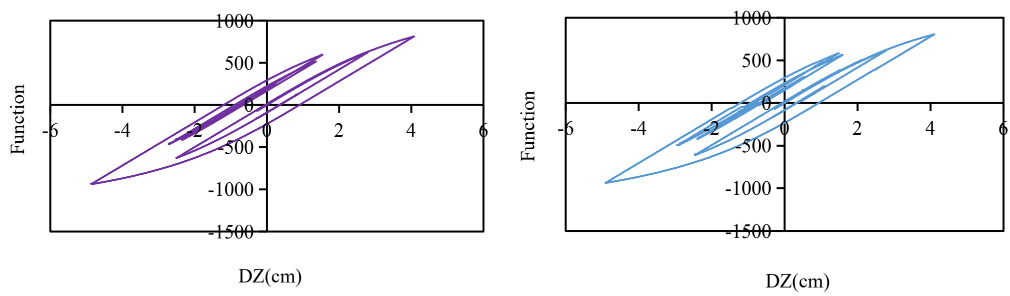

a) Condition 1 along the bridge direction excitation b) Working condition 9 combination one incentive

Fig. 11. Hysteresis curve

7. Conclusions

Nine non-isolated and earthquake-isolated structural models under different cross-bracing arrangements were established, and Elcentro seismic waves were selected. The internal force, displacement, velocity, absolute acceleration, relative acceleration, and separation of arch ribs of each model were compared and analyzed under uniform excitation along the bridge, transverse and vertical directions, multi-dimensional combined excitation, and multipoint excitation considering the traveling wave effect.

Through the above comparative analysis, we can get:

1) The main internal force of the arch ribs of the seismic isolation structure in each working

condition decreases significantly under the action of the bridge direction, the horizontal bridge direction, the combination one, and the seismic waves with different wave speeds. Under the vertical earthquake action, the arch of the seismic isolation structure, the main internal force of the rib increases. Under the action of the second combination earthquake, the axial force of the arch rib in each working condition of the seismic isolation structure decreases, the shear force F_z increases, the bending moment M_z working conditions eight and nine increase, and the rest decrease, and the combination three under the action of an earthquake, the main internal forces of the seismic isolation structure arch ribs in various working conditions have increased;

2) Under the action of transverse bridge seismic waves, the arch ribs of non-seismic and isolation models mainly undergo lateral displacement. The "K"-shaped cross brace is better than the "-" cross brace and the "meter" shape in reducing the lateral displacement of the arch rib. Transverse bracing, setting transverse bracing on the upper part of the arch rib can reduce the vertical displacement of the arch rib of the non-seismic model;

3) Under the action of transverse seismic waves, the lateral velocity of the arch ribs of the non-seismic and isolation models basically increased, and the velocity of the arch ribs of the seismic isolation structure under various working conditions decreased;

4) The "meter"-shaped cross brace at the top of the arch rib and the "K"-shaped cross brace at the lower part help reduce the lateral acceleration of the arch rib. The absolute acceleration and relative acceleration of the arch rib of the seismic isolation structure under various working conditions are significantly reduced;

5) Under the action of the maximum shear force of the seismic isolation support in the transverse direction and the combination two, working conditions 1 to 9 show a decreasing trend, and the linear directions are basically similar. In all conditions, the excitation of combination one is greater than the excitation along the bridge direction, and the cross-bridge direction and combination two are basically the same, and there is a decreasing trend from working condition one to working condition nine.

Acknowledgements

This research was funded by the Fundamental Research Funds for the Central Universities (31920210078), the National Natural Science Foundation of China (51868067).

Data availability

The datasets generated during and/or analyzed during the current study are available from the corresponding author on reasonable request.

Conflict of interest

The authors declare that they have no conflict of interest.

References

[1] Dong Rui et al., "Stability analysis of long-span CFST truss arch bridges with L-shaped bracings," (in Chinese), *China Civil Engineering Journal*, Vol. 53, No. 5, pp. 89–99, 2020.

[2] Zhang Sumei and Yun Di, "Lateral brace arrangement for large-span half-through concrete filled steel tube arch bridge," (in Chinese), *Journal of Jilin University (Engineering and Technology Edition)*, Vol. 39, No. 1, pp. 108–112, 2009.

[3] Wan Peng and Zheng Kaifeng, "The effect of end bracing location on out-of-plane ultimate bearing capacity of steel arch bridges," (in Chinese), *China Railway Science*, Vol. 27, No. 1, pp. 19–22, 2006.

[4] Jin Bo et al., "Effect of lateral brace on the stability of cable-stayed concrete filled steel tube arch bridge," (in Chinese), *Journal of Hunan University (Natural Sciences)*, Vol. 33, No. 6, pp. 6–10, 2006.

[5] Chen Baochun et al., "Application of concrete-filled steel tube arch bridges in China: current status and prospects," (in Chinese), *China Civil Engineering Journal*, Vol. 50, No. 6, pp. 50–61, 2017.

[6] Liu Zhao and Lu Zhitao, "Lateral buckling load of tied-arch bridges with transverse braces," (in Chinese), *Engineering Mechanics*, Vol. 21, No. 3, pp. 21–24, 2004.
[7] Wu Meirong et al., "Dynamic characteristics of half-through concrete-filled steel tubular arch bridges," (in Chinese), *Journal of Vibration and Shock*, Vol. 36, No. 24, pp. 85–90, 2017.
[8] Kong Dandan et al., "Influence of local instability of members on overall stability of steel truss arch bridge," (in Chinese), *Journal of Northeast Forestry University*, Vol. 49, No. 7, pp. 116–121, 2021.
[9] Li Xiayuan, Chen Jianbing, and Bao Guangming, "Comparison and selection of wind bracing reinforcement schemes for concrete-filled steel tube tied arch bridges based on dynamic characteristics," (in Chinese), *Chinese Foreign Highway*, Vol. 35, No. 1, pp. 160–165, 2015.
[10] Zheng Xiaoyan et al., "Analysis of stability and influences of temporary cross bracings of PC tied arch bridge at construction stages," (in Chinese), *Bridge Construction*, Vol. 42, No. 1, pp. 67–71, 2012.

Appendix

Table A1. Maximum internal force and shock absorption rate of arch ribs under uniform excitation

Incentive direction	Internal force	Model and shock absorption rate	Working condition								
			1	2	3	4	5	6	7	8	9
Along the bridge	Axial force Fx (kN)	Non-isolated	4534.93	4545.15	4548.65	4557.3	4551.72	4564.87	4581.32	4550.02	4555.48
		Isolated	3963.03	3982.89	3985.78	3993.48	3991.76	3998.69	4032.11	4062.09	4071.14
		Damping rate	12.61%	12.37%	12.37%	12.37%	12.30%	12.40%	11.99%	10.72%	10.63%
	Shear force Fz (kN)	Non-isolated	917.48	918.65	920.45	921.65	919.08	924.46	926.06	927.47	928.78
		Isolated	321.98	321.94	322	322.3	322.2	322.39	322.31	322.32	322.23
		Damping rate	64.91%	64.96%	65.02%	65.03%	64.94%	65.13%	65.20%	65.25%	65.31%
	Bending moment My (kN·m)	Non-isolated	3751.23	3753.01	3761.15	3762.67	3753.19	3771.23	3773.62	3778.32	3783.74
		Isolated	1387.38	1385.62	1385.54	1385.62	1386.5	1385.26	1381.31	1376.95	1375.24
		Damping rate	63.02%	63.08%	63.16%	63.17%	63.06%	63.27%	63.40%	63.56%	63.65%
Cross bridge	Axial force Fx (kN)	Non-isolated	610.05	608.91	604.5	602.52	534.59	604.95	533.73	714.06	734.57
		Isolated	273.68	273.54	272.88	272.56	256.9	268.1	297.44	653.65	658.64
		Damping rate	55.14%	55.08%	54.86%	54.76%	51.94%	55.68%	44.27%	8.46%	10.34%
	Shear force Fy (kN)	Non-isolated	180.89	189.1	183.83	190.15	103.85	164.56	142.02	232.33	237.67
		Isolated	58.55	58.98	58.85	58.37	68.37	67.78	78.18	209.98	207.11
		Damping rate	67.63%	68.81%	67.99%	69.30%	34.16%	58.81%	44.95%	9.62%	12.86%
	Bending moment Mz (kN·m)	Non-isolated	1745.89	1739.55	1741.97	1730.91	1652.05	1674.06	1560.34	2711.21	2702.32
		Isolated	1191.55	1191.33	1199.27	1199.01	1247.23	1162.67	1261.18	2908.61	2879.42
		Damping rate	31.75%	31.52%	31.15%	30.73%	24.50%	30.55%	19.17%	-7.28%	-6.55%
Vertical	Axial force Fx (kN)	Non-isolated	2895.18	2905.67	2919.86	2928.84	2942.31	2946.59	2973.49	3016.52	3021.57
		Isolated	3321.61	3321.56	3316.25	3317.23	3321.82	3309.72	3313.99	3314.5	3321.16
		Damping rate	-14.73%	-14.31%	-13.58%	-13.26%	-12.90%	-12.32%	-11.45%	-9.88%	-9.92%
	Shear force Fz (kN)	Non-isolated	337.43	340.06	334.81	337.58	343.93	332.52	338.33	339.1	342.14
		Isolated	1128.16	1129.9	1128.69	1130.91	1133.73	1130.7	1136.45	1144.87	1144.61
		Damping rate	-234.34%	-232.26%	-237.11%	-235.01%	-229.64%	-240.04%	-235.90%	-237.62%	-234.54%
	Bending moment My (kN·m)	Non-isolated	1058.7	1066.75	1049.81	1058.07	1077.95	1040.69	1058.11	1059.61	1071.18
		Isolated	4524.67	4530.19	4527.13	4534.13	4540.83	4531.31	4548.01	4569.16	4569.93
		Damping rate	-327.38%	-324.67%	-331.23%	-328.53%	-321.25%	-335.41%	-329.82%	-331.21%	-326.63%

Table A2. Maximum internal force and shock absorption rate of arch ribs under multi-dimensional excitation

Incentive direction	Internal force	Model and shock absorption rate	Working condition								
			1	2	3	4	5	6	7	8	9
Combination One	Axial force Fx (kN)	Non-isolated	4791.17	4804.44	4806.89	4820.12	4809.55	4831.38	4852.98	4819.56	4823.37
		Isolated	3970.09	3988.81	3982.47	3988.42	3989.81	4001.17	4029.14	4094.66	4109.14
		Damping rate	17.14%	16.98%	17.15%	17.25%	17.04%	17.18%	16.98%	15.04%	14.81%
	Shear force Fz (kN)	Non-isolated	934.4	935.28	936.9	937.97	932.97	938.6	937.38	937.45	940.32
		Isolated	392.63	392.79	392.58	392.1	391.28	391.64	392.56	396.52	396.88
		Damping rate	57.98%	58.00%	58.10%	58.20%	58.06%	58.27%	58.12%	57.70%	57.79%
	Bending moment My (kN·m)	Non-isolated	3752.91	3755.68	3762.75	3765.3	3749.56	3767.57	3764.34	3759	3768.39
		Isolated	1573.14	1579.72	1580.13	1579.56	1572.57	1573.99	1565.35	1590.86	1592.29
		Damping rate	58.08%	57.94%	58.01%	58.05%	58.06%	58.22%	58.42%	57.68%	57.75%
Combination Two	Axial force Fx (kN)	Non-isolated	1787.6	1798.74	1789.57	1800.25	1805.18	1853.59	1859.61	1830.46	1830.71
		Isolated	1473.47	1471.71	1481.52	1480.01	1504.23	1521.05	1555.04	1630.42	1641.37
		Damping rate	17.57%	18.18%	17.21%	17.79%	16.67%	17.94%	16.38%	10.93%	10.34%

	Shear force Fz (kN)	Non-isolated	315.01	315.52	315.25	315.71	306.88	310.96	304.47	330.04	331.77
		Isolated	354.49	355.02	354.36	355.17	365.1	364.01	372.96	402.68	405.07
		Damping rate	-12.53%	-12.52%	-12.41%	-12.50%	-18.97%	-17.06%	-22.49%	-22.01%	-22.09%
	Bending moment Mz (kN·m)	Non-isolated	1748.5	1742.22	1743.32	1732.86	1652.73	1679.33	1566.11	2713.34	2703.02
		Isolated	1188.51	1189.24	1192.43	1190.08	1240.67	1163.57	1267.35	2894.4	2845.11
		Damping rate	32.03%	31.74%	31.60%	31.32%	24.93%	30.71%	19.08%	-6.67%	-5.26%
Combination Three	Axial force Fx (kN)	Non-isolated	3295.73	3306.62	3314.77	3324.99	3318.42	3334	3359.71	3481.6	3487.94
		Isolated	3420.96	3422.17	3419.27	3420.54	3425.08	3420.04	3419.7	3432.47	3440.28
		Damping rate	-3.80%	-3.49%	-3.15%	-2.87%	-3.21%	-2.58%	-1.79%	1.41%	1.37%
	Shear force Fz (kN)	Non-isolated	441.19	444.38	439.01	442.11	450.47	440.65	449.68	459	462.19
		Isolated	1140.53	1142.15	1140.91	1146.34	1149.59	1146.78	1152.87	1169.45	1169.17
		Damping rate	-158.51%	-157.02%	-159.88%	-159.29%	-155.20%	-160.25%	-156.38%	-154.78%	-152.96%
	Bending moment My (kN·m)	Non-isolated	1428.57	1440.89	1431.49	1444.06	1455.82	1436.77	1459.4	1511.04	1505.11
		Isolated	4494.48	4500.12	4497.68	4507.43	4519.6	4512.9	4533.85	4585.72	4591
		Damping rate	-214.61%	-212.32%	-214.20%	-212.14%	-210.45%	-214.10%	-210.67%	-203.48%	-205.03%

Table A3. The maximum internal force and shock absorption rate of arch ribs considering traveling wave effect

Wave speed/(m/s^2)	Internal force	Model and shock absorption rate	Working condition								
			1	2	3	4	5	6	7	8	9
100	Axial force Fx (kN)	Non-isolated	3852.42	3856.42	3857.74	3860.85	3861.33	3863.93	3870.79	3880.93	3883.24
		Isolated	520.67	522.55	522.37	523.81	523.73	523.75	526.45	528.48	529.06
		Damping rate	86.48%	86.45%	86.46%	86.43%	86.44%	86.45%	86.40%	86.38%	86.38%
	Shear force Fz (kN)	Non-isolated	1666.51	1667.43	1667.71	1668.71	1667.33	1672.1	1671.72	1673.34	1674.12
		Isolated	171.41	171.16	171.01	170.66	170.93	170.62	170.02	169.87	170.04
		Damping rate	89.71%	89.74%	89.75%	89.77%	89.75%	89.80%	89.83%	89.85%	89.84%
	Bending moment My (kN·m)	Non-isolated	6876.43	6880.55	6882.39	6886.51	6881.43	6897.96	6902.4	6910.57	6913.85
		Isolated	546.41	546.86	547.49	547.27	547.35	548.28	548.97	550.39	551.68
		Damping rate	92.05%	92.05%	92.05%	92.05%	92.05%	92.05%	92.05%	92.04%	92.02%
200	Axial force Fx (kN)	Non-isolated	4199.8	4206.56	4207.83	4213.32	4214.77	4219	4231.08	4245.63	4248.93
		Isolated	749.72	753.1	753.01	757.06	757.83	750.79	758.66	758.81	760.53
		Damping rate	82.15%	82.10%	82.10%	82.03%	82.02%	82.20%	82.07%	82.13%	82.10%
	Shear force Fz (kN)	Non-isolated	1273.92	1276.09	1274.96	1275.59	1275.48	1275.28	1278.56	1280.12	1280.2
		Isolated	155.23	155.13	154.98	154.57	154.21	154.55	153.92	153.14	153.23
		Damping rate	87.81%	87.84%	87.84%	87.88%	87.91%	87.88%	87.96%	88.04%	88.03%
	Bending moment My (kN·m)	Non-isolated	4950.38	4954.86	4955.16	4960.66	4963.35	4960.57	4973.22	4983.6	4987.3
		Isolated	586.18	585.33	585.73	585.37	585.12	585.77	585.04	584.47	583.99
		Damping rate	88.16%	88.19%	88.18%	88.20%	88.21%	88.19%	88.24%	88.27%	88.29%
300	Axial force Fx (kN)	Non-isolated	3325.7	3329	3328.98	3330.66	3334.49	3337.37	3339.91	3345.95	3346.56
		Isolated	804.53	806.12	805.87	809.03	809.83	808.14	814.24	809.7	811.4
		Damping rate	75.81%	75.78%	75.79%	75.71%	75.71%	75.79%	75.62%	75.80%	75.75%
	Shear force Fz (kN)	Non-isolated	1250.91	1255.81	1255.42	1258.82	1257.02	1260.33	1267.79	1269.53	1269.93
		Isolated	138.13	137.35	137.37	137.26	137.97	137.26	136.99	137.2	136.96
		Damping rate	88.96%	89.06%	89.06%	89.10%	89.02%	89.11%	89.19%	89.19%	89.22%
	Bending moment My (kN·m)	Non-isolated	4614.67	4626.32	4623.44	4635.08	4634.55	4642.87	4662.47	4674.2	4678.59
		Isolated	554.55	553.44	553.61	552.55	553.12	552.87	550.52	549.09	548.25
		Damping rate	87.98%	88.04%	88.03%	88.08%	88.07%	88.09%	88.19%	88.25%	88.28%
400	Axial force Fx (kN)	Non-isolated	2001.98	2000.47	2001.26	1998.17	2002.35	2002.54	1992.68	2002.4	2004.08
		Isolated	866.69	869.49	871.78	872.87	870.94	873.89	878	869.54	870.4
		Damping rate	56.71%	56.54%	56.44%	56.32%	56.50%	56.36%	55.94%	56.58%	56.57%
	Shear force Fz (kN)	Non-isolated	1078.69	1081.48	1080.86	1082.59	1082.04	1082.67	1087.95	1090.47	1090.65
		Isolated	129.81	129.65	129.76	129.77	129.79	129.92	129.94	129.83	129.74
		Damping rate	87.97%	88.01%	87.99%	88.01%	88.01%	88.00%	88.06%	88.09%	88.10%
	Bending moment My (kN·m)	Non-isolated	4306.38	4314.78	4312.4	4319.56	4318.96	4322.06	4335.74	4342.61	4346.3
		Isolated	594.91	593.36	593.44	592.71	592.7	592.87	591.49	589.37	588.43
		Damping rate	86.19%	86.25%	86.24%	86.28%	86.28%	86.28%	86.36%	86.43%	86.46%
500	Axial force Fx (kN)	Non-isolated	2173.11	2173.33	2175.69	2176.14	2176.43	2179.8	2183.08	2190.55	2193.51
		Isolated	902.19	904.35	906.2	908.96	907.2	909.61	915.2	906.55	907.67
		Damping rate	58.48%	58.39%	58.35%	58.23%	58.32%	58.27%	58.08%	58.62%	58.62%
	Shear force Fz (kN)	Non-isolated	1050.06	1051.37	1051.48	1052.65	1052.65	1053.31	1056.31	1059.72	1060.98
		Isolated	136.03	135.93	136.09	136.04	135.95	136.22	136.15	136.12	136
		Damping rate	87.05%	87.07%	87.06%	87.08%	87.08%	87.07%	87.11%	87.16%	87.18%
	Bending moment My (kN·m)	Non-isolated	4331.32	4337.84	4337.69	4343.13	4343.31	4345.57	4357.41	4369.91	4374.32
		Isolated	630.5	629.46	629.57	628.67	628.26	628.83	627.11	624.63	623.57
		Damping rate	85.44%	85.49%	85.49%	85.52%	85.53%	85.53%	85.61%	85.71%	85.74%

1000	Axial force Fx (kN)	Non-isolated	3678.94	3686.52	3686.98	3696.27	3691.74	3702.87	3708.38	3693.45	3698.67
		Isolated	943.16	947.1	948.88	951.56	949.69	952.31	959.51	954.69	955.7
		Damping rate	74.36%	74.31%	74.26%	74.26%	74.28%	74.28%	74.13%	74.15%	74.16%
	Shear force Fz (kN)	Non-isolated	1047.8	1049.53	1051.06	1051.77	1049.13	1053.82	1056.15	1057.85	1059
		Isolated	122.84	122.72	122.87	122.81	122.77	122.97	122.89	122.73	122.68
		Damping rate	88.28%	88.31%	88.31%	88.32%	88.30%	88.33%	88.36%	88.40%	88.42%
	Bending moment My (kN·m)	Non-isolated	3010.44	3017.31	3017.79	3023.91	3023.88	3028.34	3039.98	3052.94	3060.72
		Isolated	545.06	543.27	543.47	542.33	542.69	542.49	540.13	537.36	537.04
		Damping rate	81.89%	81.99%	81.99%	82.07%	82.05%	82.09%	82.23%	82.40%	82.45%
1500	Axial force Fx (kN)	Non-isolated	4161.2	4170.73	4171.33	4180.59	4174.41	4188.64	4208.25	4177.41	4182.35
		Isolated	952.21	955.48	957.44	960.84	958.89	961.24	968.91	964.19	964.67
		Damping rate	77.12%	77.09%	77.05%	77.02%	77.03%	77.05%	76.98%	76.92%	76.93%
	Shear force Fz (kN)	Non-isolated	1034.8	1036.54	1038.39	1039.2	1036.35	1041.68	1043.97	1045.2	1046.49
		Isolated	118.28	118.13	118.42	118.28	118.1	118.56	118.4	118.18	118.02
		Damping rate	88.57%	88.60%	88.60%	88.62%	88.60%	88.62%	88.66%	88.69%	88.72%
	Bending moment My (kN·m)	Non-isolated	2794.08	2795.7	2803.14	2804.7	2797.28	2812.77	2814.72	2817.44	2821.68
		Isolated	514.34	513.03	513.17	511.76	511.93	512.02	509.32	506.77	505.42
		Damping rate	81.59%	81.65%	81.69%	81.75%	81.70%	81.80%	81.91%	82.01%	82.09%
2000	Axial force Fx (kN)	Non-isolated	4256.85	4266.21	4268.61	4278.59	4270.5	4286.33	4304.75	4271.53	4275.49
		Isolated	957.38	960.88	962.69	966.05	964.39	966.47	974.28	967.76	968.47
		Damping rate	77.51%	77.48%	77.45%	77.42%	77.42%	77.45%	77.37%	77.34%	77.35%
	Shear force Fz (kN)	Non-isolated	1034.68	1036.26	1038.02	1039.02	1036.28	1041.59	1043.68	1044.77	1045.99
		Isolated	118.69	118.49	118.79	118.67	118.48	118.93	118.8	118.62	118.47
		Damping rate	88.53%	88.57%	88.56%	88.58%	88.57%	88.58%	88.62%	88.65%	88.67%
	Bending moment My (kN·m)	Non-isolated	2914.52	2915.8	2923.91	2925.29	2917.29	2933.72	2935.28	2938.24	2942.97
		Isolated	516.22	514.7	514.84	513.5	513.82	513.82	511.34	508.87	507.44
		Damping rate	82.29%	82.35%	82.39%	82.45%	82.39%	82.49%	82.58%	82.68%	82.76%

Zhonghu Gao received master's degree in school of civil engineering from Lanzhou University of Technology, Lanzhou, Gansu, China, in 2012. Now he works at Northwest Minzu university. His current research interests include structural anti-seismic, seismic mitigation and isolation control.

Weigang Sun received Ph.D. degree in Highway School from Chang'an University, Xi'an, Shaanxi, China, in 2016. His current research interests include damage identification and condition assessment of bridge structure, mechanical behavior of truss bridge and bridge health monitoring.